Geophysical Research Letters

RESEARCH LETTER
10.1029/2018GL080042

Key Points:
- Long-period Love wave radiation patterns have acute sensitivity to dip for shallow thrust events with shallowly dipping (<10 degrees) faults
- Love waves with a period of 227.56 s indicate an average dip of 2.0 degrees to 5.0 degrees for the 2010 Mentawai near-trench tsunami earthquake
- Love waves with a period of 204.80 s indicate a dip of 2.5–7.5 degrees for the 4 May 2018 Hawaii Island basal decollement earthquake

Supporting Information:
- Supporting Information S1

Correspondence to:
T. Lay,
tlay@ucsc.edu

Citation:
Lay, T., Ye, L., Kanamori, H., & Satake, K. (2018). Constraining the dip of shallow, shallowly dipping thrust events using long-period Love wave radiation patterns: Applications to the 25 October 2010 Mentawai, Indonesia, and 4 May 2018 Hawaii Island earthquakes. *Geophysical Research Letters*, *45*, 10,342–10,349. https://doi.org/10.1029/2018GL080042

Received 13 AUG 2018
Accepted 17 SEP 2018
Accepted article online 21 SEP 2018
Published online 7 OCT 2018

Constraining the Dip of Shallow, Shallowly Dipping Thrust Events Using Long-Period Love Wave Radiation Patterns: Applications to the 25 October 2010 Mentawai, Indonesia, and 4 May 2018 Hawaii Island Earthquakes

Thorne Lay[1], Lingling Ye[2,3], Hiroo Kanamori[4], and Kenji Satake[3]

[1]Department of Earth and Planetary Sciences, University of California, Santa Cruz, CA, USA, [2]Guangdong Provincial Key Lab of Geodynamics and Geohazards, School of Earth Sciences and Engineering, Sun Yat-sen University, Guangzhou, China, [3]Earthquake Research Institute, University of Tokyo, Tokyo, Japan, [4]Seismological Laboratory, California Institute of Technology, Pasadena, CA, USA

Abstract Constraining precise faulting geometry for shallow, shallowly dipping thrust earthquakes is a common challenge. Plate boundary megathrust faults near the trench and décollement faults beneath volcanic islands and nappes may dip only a few degrees. Long-period point source moment tensor waveform inversions provide limited resolution of shallow fault dip angle. The possibility of splay faulting requires precise dip estimation. High sensitivity to dip is provided by long-period Love wave amplitude azimuthal radiation patterns, which undergo rapid change from four lobed to two lobed as dip decreases from 10° to 0°. Modeling variability in Love wave nodal amplitudes allows the dip to be determined to within a few degrees. This is demonstrated for the 25 October 2010 Mentawai (M_{WW} 7.8) tsunami earthquake, which ruptured the 2.0–5.0° dipping megathrust beneath the shallow sedimentary wedge offshore of Indonesia, and the 4 May 2018 Hawaii Island (M_{WW} 6.9) thrust earthquake, which ruptured the 2.5–7.5° dipping décollement under the island flank.

Plain Language Summary Earthquakes that involve thrust faulting at shallow depth occur commonly, and determining the fault dip angle is important for interpreting the nature of such events. Routine seismic wave analysis procedures for determining the faulting geometry for shallow thrust events often do not provide precise resolution of dip, leaving ambiguity in the assessment of the tectonic nature of the event. Spectral analysis of long-period radiation patterns for Love waves provides good sensitivity to fault dip angle for large shallow, shallowly dipping thrust events. Analysis of long-period surface waves for two shallow thrust events, a large near-trench subduction zone *tsunami earthquake* and the other a large earthquake at the base of the island mass of Hawaii, demonstrates that fault dip can be resolved to within a few degrees based on the sensitivity of Love wave radiation patterns to dip angle. Improved resolution of dip angle provides better confidence in the tectonic interpretation and improves seismic moment and slip estimation.

1. Introduction

Thrust faulting occurs on very shallowly dipping fault planes in multiple environments. Subduction zone plate boundary megathrust faults have very low dip angles, often <5°, located below the toe of the sedimentary wedge near the trench (e.g., Hayes et al., 2012). It is now recognized that large megathrust earthquakes can involve slip that extends to the trench, notably in tsunami earthquakes (e.g., Ammon et al., 2006; Bilek & Lay, 2002; Kanamori, 1972; Polet & Kanamori, 2000). Volcanic islands superimposed on depressed oceanic seafloor can produce shallowly dipping thrust faulting on the basal décollement as topographic stresses and magma injection drive the island to spread (e.g., Day et al., 2005; Gillard et al., 1996; Swanson et al., 1976). Nappes, or thrust sheets, in continental regions commonly involve décollement with very low (<5°) dip angles. With subduction zone megathrusts and island décollement seismogenic environments both usually being located offshore, seismic waves are the primary data available to determine faulting geometry and slip distribution for such shallow thrust earthquakes. The widespread occurrence of splay faulting in upper wedges with dip angles significantly larger than the megathrust (e.g., Heidarzadeh, 2011; Park et al., 2002; Plaza-Faverola et al., 2016) motivates reliable determination of earthquake dip rather than assumption of megathrust geometry.

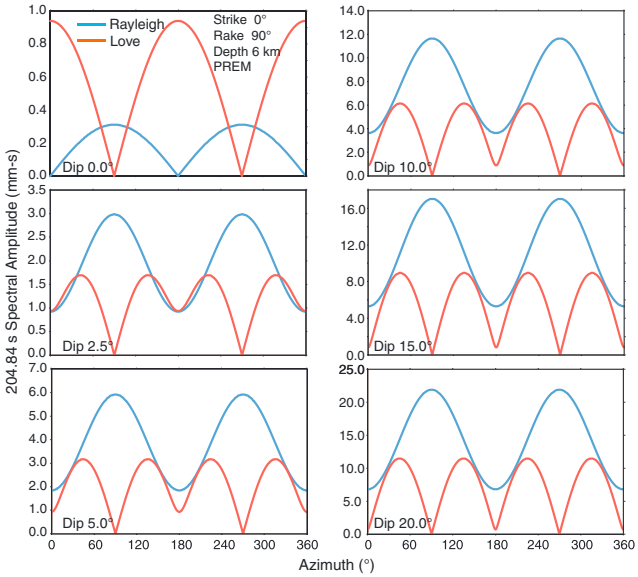

Figure 1. Rayleigh wave (blue) and Love wave (red) azimuthal amplitude radiation patterns for period, $T = 204.84$ s for point source step function double couples 6 km deep in the Preliminary Reference Earth Structure (PREM) structure, with strike $\phi = 0°$, rake $\lambda = 90°$, seismic moment $M_0 = 1.0 \times 10^{20}$ Nm, and dip δ varying from 0° to 20°. Note variation in vertical scales.

Uncertainty in fault plane dip, δ, produces substantial uncertainty in estimated seismic moment (M_0) and inferred slip for shallow thrust events. Excitation and radiation patterns for Rayleigh and Love waves are proportional to $M_0 \sin(2\delta)$ for shallow dip-slip dislocations due to vanishing of vertical strains at the free surface (e.g., Kanamori & Given, 1981). Dip angle also controls vertical seafloor displacement, hence tsunami generation. Routine waveform-based point source moment tensor inversions using long-period seismic waves provide limited resolution (with at least ±10° uncertainty) of fault dip as it decreases below 15°. Dip resolution is comparably poor in finite-fault inversions based on teleseismic body waves, so a priori geometry of the thrust plane is typically assumed. Even for major (M_W 7.0 to 8.0) thrust earthquakes at shallow depths, such as tsunami earthquakes, teleseismic wave analysis of the mainshock radiation alone provides limited resolution of the near-trench faulting geometry (e.g., Lay et al., 2011). This remains the case even when seismic, on-land geodetic, and tsunami data are analyzed together (e.g., Yue et al., 2014).

Somewhat surprisingly, perhaps the most sensitive readily observable seismic radiation characteristic that can tightly constrain shallow, shallowly dipping thrust fault dip for large earthquakes is provided by long-period Love wave amplitude radiation patterns. This arises due to a rapid change in the azimuthal radiation pattern from quasi four lobed for dips larger than 10° to two lobed for dips less than 2°. Rayleigh and Love wave amplitude radiation patterns for a period $T = 204.84$ s for 6-km-deep point source dip-slip shear dislocations with varying dip in the Preliminary Reference Earth Model (PREM) structure (Dziewonski & Anderson, 1981) are shown in Figure 1. The seismic moment is the same in each case, so the much stronger signal generation for steeper dip is apparent. Essentially, the two Love wave radiation nodes along the fault strike for steeper dip geometry become lobes in the radiation pattern for zero dip. There is a corresponding rapid decrease in Rayleigh wave amplitudes relative to Love wave amplitudes, and deepening of Rayleigh wave nodes along strike. This behavior is expected over a broad long-period range, corresponding to that for surface wave periods typically analyzed for large earthquakes. As source depth increases, the sensitivity to dip angle also increases, as shown in supporting information Figure S1. For source depths of 9 to 15 km, slight (~2.5°) increase in dip angle produces Love wave radiation patterns similar to those for smaller dip at 6-km depth. The Love wave radiation pattern is insensitive to rake variations of ±30° from purely dip slip (Figure S2). We do not focus on the surface wave phase behavior here, as it is primarily sensitive to source duration and depends on having path-specific propagation corrections. This behavior has long been known and has given rise to ambiguity in interpretation of possible horizontal point force excitation of seismic waves from landslides versus very shallow low-angle dip-slip faulting, because both produce rare two-lobed Love wave radiation patterns (e.g., Dahlen, 1993; Eissler & Kanamori, 1987; Kanamori & Given, 1982; Kawakatsu, 1989; Wyss & Kovach, 1988). Here we exploit this acute sensitivity to dip of long-period Love waves for shallow, shallowly dipping thrust events to constrain the faulting geometries of two large events in different tectonic domains, assessing the implications for seismic moment and slip estimation, along with tectonic interpretation of the faulting.

2. Data and Procedure

Two shallow focus dip-slip earthquakes are considered to demonstrate the dip resolution provided by long-period Love wave radiation patterns. The first is the 25 October 2010 Mentawai tsunami earthquake (U.S. Geological Survey [USGS]-National Earthquake Information Center: 14:42:22 UTC, 3.487°S, 100.082°E, M_{WW} 7.8; https://earthquake.usgs.gov/earthquakes/eventpage/usp000hnj4#executive). The *W*-phase moment tensor for this event (Duputel et al., 2012) has a best double couple with strike $\phi = 324°$, dip $\delta = 8°$, rake $\lambda = 96°$, seismic moment $M_0 = 5.41 \times 10^{20}$ Nm, and half duration of 38 s. The global centroid moment tensor (GCMT) best double-couple solution (http://www.globalcmt.org/CMTsearch.html) has $\phi = 316°$, $\delta = 8°$, $\lambda = 96°$, $M_0 = 6.77 \times 10^{20}$ Nm, and 37.3-s centroid time. The rupture process of this event has been extensively studied (e.g., Hill et al., 2012; Lay et al., 2011; Newman et al., 2011; Satake et al., 2013; Yue et al., 2014), and seismic

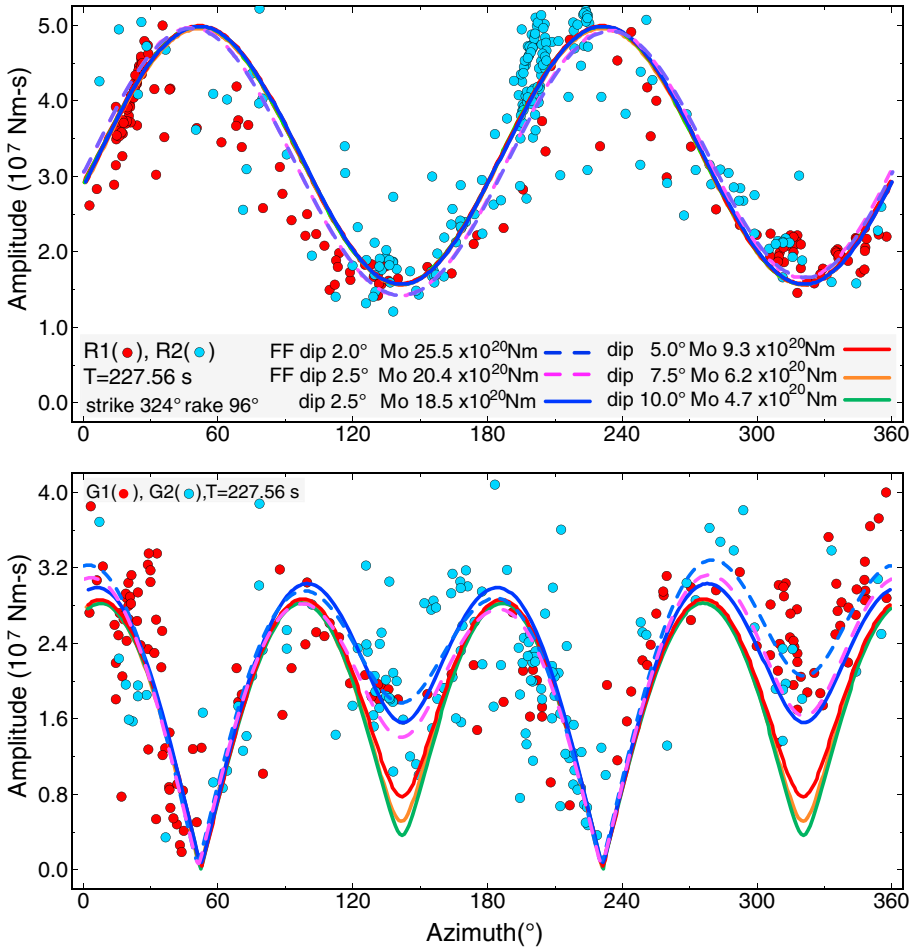

Figure 2. Observed and predicted Rayleigh wave (top) and Love wave (bottom) source spectral amplitudes for $T = 227.56$ s for the 25 October 2010 Mentawai tsunami earthquake. Red dots indicate short-arc (R1, G1) observations; cyan dots indicate long-arc (R2, G2) observations. Theoretical amplitudes for models with $\phi = 324°$, $\lambda = 96°$, and δ varying from 2° to 10° are shown by the color curves. Seismic moment for each model is adjusted to give the same Rayleigh wave peak amplitude. All models have step function displacement time history except those labeled with FF, which are finite-fault models with 100-km unilateral rupture along strike with $V_r = 1.8$ km/s and particle displacement times of 10 s.

reflection profiles indicate the dip of the megathrust is about 7.5° from the hypocenter to the trench (Singh et al., 2011), consistent with the dip for the long-period moment tensors.

The second event is the significantly smaller 4 May 2018 Hawaii Island earthquake (USGS-National Earthquake Information Center, 22:32:54 UTC, 19.313°N, 154.998°W, M_{WW} 6.9; https://earthquake.usgs.gov/earthquakes/eventpage/us1000dyad#executive), which occurred early in the 2018 Kilauea eruption sequence. The USGS *W*-phase best double-couple solution has $\phi = 240°$, $\delta = 20°$, $\lambda = 114°$, $M_0 = 2.74 \times 10^{19}$ Nm, and half duration of 6.5 s, while the GCMT solution has $\phi = 245°$, $\delta = 20°$, $\lambda = 120°$, $M_0 = 2.71 \times 10^{19}$ Nm, and 14.7 s centroid time. Finite-fault models of this event have been obtained by Liu et al. (2018) and Bai et al. (2018). It occurred beneath the offshore flank of Kilauea seaward of the East Rift Zone. If the long-period estimates of dip are too large, it plausibly ruptured the ~4° dipping décollement between the island mass and the former Pacific plate seafloor as the flank wedge moves seaward (e.g., Delaney et al., 1998; Denlinger & Okubo, 1995; Morgan et al., 2000; Morgan et al., 2003). Both of these dip-slip earthquakes appear to have ruptured at very shallow depth (nominal long-period centroid depths are ~11.5 km), with primary slip from 0 to 10 km below the seafloor.

Long 1-s sampled (LH) three-component seismograms from global digital networks are obtained for both events from the Incorporated Research Institutions for Seismology Data Management System. Vertical

components are used for Rayleigh waves, and horizontal components are rotated to separate Love waves. Spectra are computed for group velocity-windowed R1, R2, G1, and G2 arrivals and corrected for propagation effects to obtain source spectra using standard processing (e.g., Kanamori & Given, 1981; Velasco et al., 1992; Zhang & Lay, 1990). Such spectral measurements can be inverted for the source moment tensor, but our goal here is to focus on the Rayleigh and Love wave amplitude radiation patterns to evaluate their sensitivity to dip, motivated by Figure 1.

3. Results for the 2010 Mentawai Earthquake

The Rayleigh and Love wave source spectra for a period of 227.56 s for the 2010 Mentawai earthquake are shown in Figure 2, plotted versus azimuth from the source. The short-arc (R1, G1) and long-arc (R2, G2) arrivals give generally compatible source spectrum estimates, and there is typical moderate level of scatter due to use of simplified geometric spreading and attenuation corrections. A cluster of anomalously low R1 amplitudes at North American stations for azimuths of 30° to 40° was removed, as the spectra appear to have destructive interference from a 3-D propagation effect in the Pacific Ocean. The source spectra show the two-lobed radiation pattern for the Rayleigh waves and a quasi-four-lobed pattern for the Love waves, as expected for a shallowly dipping thrust event. Theoretical source spectra for $\phi = 324°$, $\lambda = 96°$, and variable δ from 2.5° to 10° computed for point sources 6 km deep in the PREM structure, which has a 3-km-deep ocean layer, are shown by solid lines. The seismic moments for the theoretical spectra are scaled to give the same peak amplitude for the Rayleigh waves, and the point source calculations exactly overlap. Note that the Love wave nodes near azimuths of 120–160° and 300–340° are not as pronounced as those near 50° and 230°, and this is accounted for by having dip less than 5°. There is also slight enhancement of both Rayleigh and Love wave nodal amplitudes at azimuths of ~330° relative to ~150°, which is consistent with unilateral rupture extending along strike for about 100 km at a rupture velocity $V_r = 1.8$ km/s (Yue et al., 2014), as shown by the theoretical spectra for finite-fault models for $\delta = 2.0°$ and 2.5°. Overall, the spectra are compatible with $\delta = 2.0°$ to 5°, with seismic moments increased relative to that for a dip of 7.5°, as used by Yue et al. (2014). Similar results are found for other frequencies.

Because the 2010 Mentawai event has relatively long source duration, typical of a tsunami earthquake, source finiteness corrections are needed for precise seismic moment estimation, but the asymmetry of the Love wave radiation nodes can be characterized even with the step dislocation point source calculations. Scatter of near-nodal observations, particularly for the phase (not shown), makes formal inversion of the spectra rather unstable, and least squares estimates tend to emphasize the large-amplitude data. Here the forward models of the spectra directly guide selection of reasonable fault dip based on matching the radiation asymmetry. Standard long-period waveform inversions tend to not resolve subtle variations in relative nodal patterns like those seen in Figure 2, so it is not surprising that they obtain a steeper dip than the optimal value indicated by spectra. The advantage of spectral analysis is that radiation pattern nodes are clearly observed and can be properly weighted, as long as enough data are available to sample the full pattern well.

4. Results for the 2018 Hawaii Island Earthquake

Rayleigh and Love wave source spectra for a period of 204.80 s for the 2018 Hawaii earthquake are shown in Figure 3, along with predictions for step function dislocation point sources for $\phi = 235°$, $\lambda = 102°$, and δ varying from 2.5° to 12.5°. The theoretical models are again scaled to have the same peak Rayleigh wave radiation, so the Rayleigh wave curves overlap. The scatter is somewhat higher than for the larger 2010 event, but the two-lobed pattern for the Rayleigh waves is clear and the Love wave radiation pattern is quasi four lobed, with the nodes near 50° and 230° azimuth being less pronounced than those near 140° and 320°. While instrument calibration at long period is always a concern, the stability of the Rayleigh wave spectra and omission of Love wave spectra that have inconsistent short-arc and long-arc arrivals provide confidence in the observations. Focusing and defocusing of Love waves, which sample shallower lithosphere than Rayleigh waves, likely accounts for the greater scatter of the former. The models indicate that the asymmetry in the Love wave radiation nodes is well accounted for by values of dip from 2.5° to 7.5° (allowing for some uncertainty in source depth guided by Figure S1). Shallower dip angles ($<2°$) decrease the Rayleigh to Love wave ratio rapidly, at odds with the data. These dips are significantly less than the 20° value for the *W*-phase and GCMT

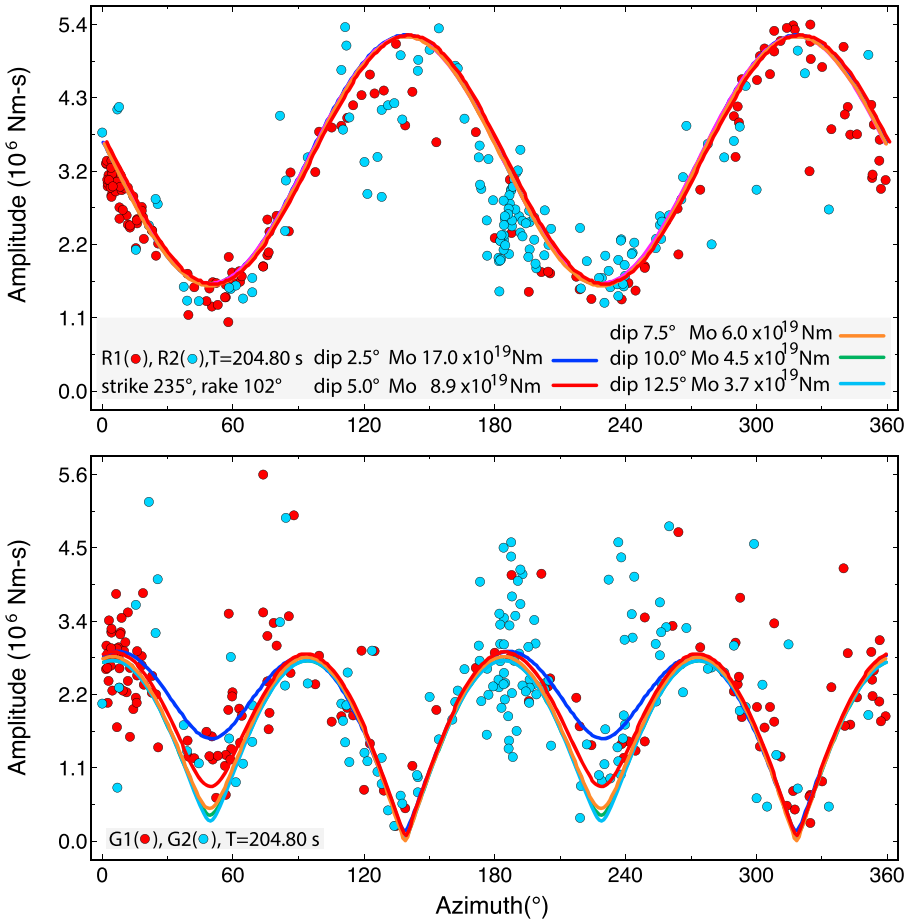

Figure 3. Observed and predicted Rayleigh wave (top) and Love wave (bottom) source spectral amplitudes for $T = 204.80$ s for the 4 May 2018 Hawaii Island earthquake. Red dots indicate short-arc (R1, G1) observations; cyan dots indicate long-arc (R2, G2) observations. Theoretical amplitudes for point source models with step function displacement time histories with $\phi = 235°$, $\lambda = 102°$, and δ from 2.5° to 12.5° are shown by the color curves. Seismic moment for each model is adjusted to give the same Rayleigh wave peak amplitude.

solutions, which predict very pronounced and symmetric nodes in the Love wave radiation pattern (e.g., Figure 1).

Given that there will be a noise threshold in the spectral data, perfect nodes are not expected to be observed, so it is the systematic difference in the nodes along the rupture direction versus those in the perpendicular direction that should be focused on. The amplitude ratio of the peak Rayleigh waves to the peak Love waves is relatively insensitive to dip but can be influenced by source depth and velocity structure for the excitation kernels. This allows a range of possible dip of from 2.5° to 7.5° for this event; these values are much smaller than typically expected for a splay fault, so the constraint is very useful for tectonic interpretation.

5. Discussion and Conclusions

The long-period Love wave spectra for the 2010 Mentawai and 2018 Hawaii events indicate shallow dip for the primary surface wave generation in both cases. As a result, steeper dipping splay faults in the overthrust wedges can be ruled out as having produced the primary long-period radiation for both earthquakes. We cannot resolve whether secondary radiation from steeper splay faulting contributed in each case, but it will not account for the Love wave radiation pattern. It is straightforward to implement this analysis of long-period source spectra to supplement waveform-based long-period moment tensor inversions to better constrain the geometry for finite-fault inversions. Sufficient generation of long-period surface waves with good

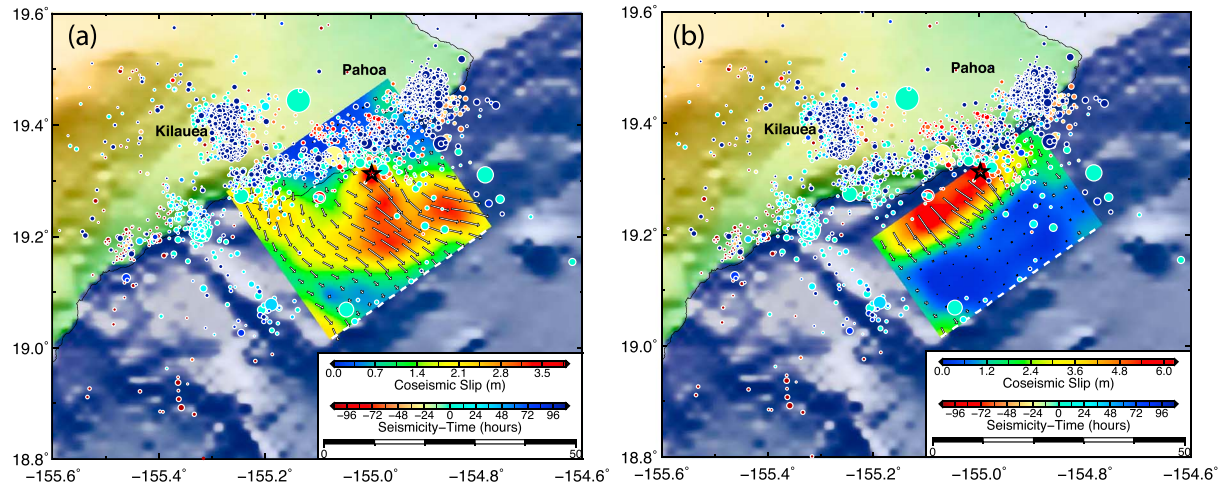

Figure 4. Finite-fault slip inversions using teleseismic broadband *P* and *SH* waves for the 4 May 2018 Hawaii Island earthquake for (a) $\phi = 235°$ and $\delta = 7.5°$, constrained to fit onshore GPS data and regional tsunami recordings (Bai et al., 2018), and (b) $\phi = 235°$ and $\delta = 3.0°$ constrained to fit the GPS data. The inversion in (a) gives $M_0 = 8.7 \times 10^{19}$ Nm (M_W 7.2), while that in (b) gives $M_0 = 7.5 \times 10^{19}$ Nm (M_W 7.2). U.S. Geological Survey catalog seismicity from 11 April to 14 May is shown by time-coded circles. Subfault slip direction and magnitude are indicated by arrows (direction of hanging wall movement). The black star indicates the 2018 event epicenter. The faults dip gently toward the northwest and are likely the basal décollement between the volcanic mass and the former Pacific seafloor. Inferred slip distribution and seismic moment depend on the dip angle estimate, so precise estimation is important.

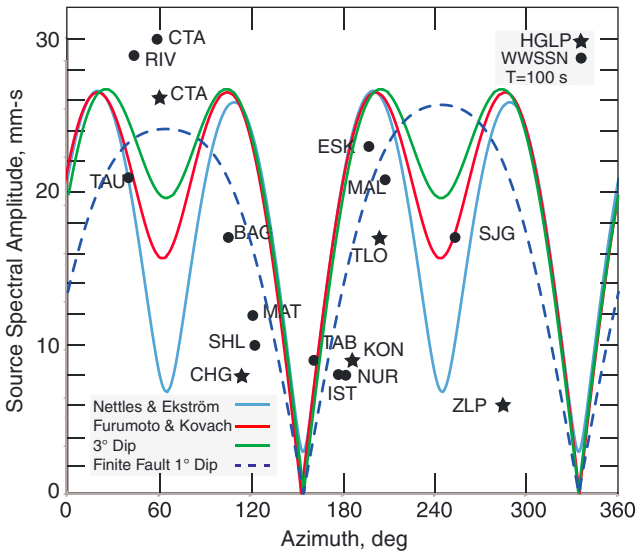

Figure 5. Observed and theoretical Love wave source spectra for $T = 100$ s for the 1975 Kalapana, Hawaii, earthquake. The observed spectra (G2 spectra from Eissler & Kanamori, 1987) are from WWSSN analog stations (black circles) or HGLP digital stations (black stars). Solid curves are theoretical spectra for point source step function displacement models at 6-km depth in the Preliminary Reference Earth Structure (PREM) structure. The blue curve is for the centroid moment tensor solution of Nettles and Ekström (2004), with $\phi = 266°$, $\delta = 9°$, $\lambda = 133°$, and $M_0 = 3.8 \times 10^{20}$ Nm. The red curve is for a solution of Furumoto and Kovach (1979), with $\phi = 244°$, $\delta = 9°$, $\lambda = 90°$, and $M_0 = 7.95 \times 10^{20}$ Nm. The green curve has $\phi = 244°$, $\delta = 3°$, $\lambda = 90°$, and $M_0 = 9.9 \times 10^{20}$ Nm. The dashed curve is for a finite bilateral rupture model extending 32 km along positive strike direction and 24 km along negative strike direction with $\phi = 244°$, $\delta = 1°$, $\lambda = 90°$, and $M_0 = 16 \times 10^{20}$ Nm, $V_r = 1.5$ km/s, and 30 s particle dislocation time. WWSSN = World-Wide Standardized Seismograph Network; HGLP = High-Gain Long Period Network.

azimuthal coverage is required for this method to be applied, so it is most viable for events with magnitudes of 6.5 and larger.

There are important implications of the fault dip being shallower than indicated by point source moment tensor inversions for these large thrust events. Since long-period estimates of seismic moment increase as the dip decreases, for both events here the seismic moment is likely higher than has been inferred previously. Estimates of slip from seismic inversions depend on seismic moment and assumed rigidity, so it is also possible that slip is larger than previously inferred. However, for both events, previous finite-fault models using fairly shallow dip (~7.5°) have been constrained by geodetic and tsunami observations that are directly sensitive to slip; thus, very large increases in slip are unlikely. Shallower dip will typically reduce tsunami excitation, so self-consistent calculations need to be made to ensure that seismic moment and dip are compatible with observed signals. For the 2010 Mentawai event, slip may extend under nearly horizontal sediments seaward of the deformation front, but small pop-up structures may contribute to tsunami excitation.

For the 2018 Hawaii Island earthquake, Figure 4 compares slip models obtained from inversion of broadband teleseismic *P* and *SH* waves assuming a dip of 7.5° (Bai et al., 2018) and a slightly perturbed inversion of the same data for a dip of 3.0°. For the 7.5° dip case, the model was shown to be consistent with regional GPS and tsunami observations. The spatial distribution of slip is dependent on the assumed dip; there is a landward shift of slip for the 3° dip model. The fit to the seismic data and GPS observations is not quite as good for the latter model; exploration of effects of assumed hypocentral depth, rupture dimensions, rupture velocity, etc., may allow a model with 3° dip to match all data as well as found for the steeper dip by Bai et al. (2018). The seismic moment for the 3° dip model is actually slightly smaller than for 7.5° dip; a large increase in moment is not required for fitting the body waves. Reflection profiles of the island

flank are consistent with a basal décollement dip of from 3° to 5°, but the structure is variable and locally may be flatter or steeper (Morgan et al., 2003; Park et al., 2007). Slip on this shallow décollement has been proposed for much larger events in Hawaii, such as the great 1868 rupture (Wyss, 1988), and the 1975 Kalapana event (e.g., Furumoto & Kovach, 1979).

The 1975 Kalapana, Hawaii, earthquake ruptured the same region as the 2018 event, with very similar epicenter. The 1975 event was much larger, but there is similar uncertainty in faulting orientation, compounded by significant coastal slumping. Ando (1979) initially interpreted the event as a shallowly dipping (10°) normal fault at shallow depth, while Furumoto and Kovach (1979) argued for a shallowly dipping (9°) thrust event on the same décollement as that which ruptured in 2018. Based on lack of a clear four-lobed pattern in 100-s period Love wave (G2) spectral amplitudes (Figure 5) along with evidence of shallow coastal slumping, Eissler and Kanamori (1987) interpreted the Kalapana source with a single-force model appropriate for a disaggregated landslide. This produces a two-lobed Love wave radiation pattern. In contrast, Nettles and Ekström (2004) obtained a centroid moment tensor thrust fault solution with $\delta = 9°$.

Love wave ($T = 100$ s) observations (from Eissler & Kanamori, 1987) and step dislocation radiation patterns are shown in Figure 5 for dip angle δ ranging from 1° to 9°. The radiation pattern for the relatively oblique ($\lambda = 133°$) centroid moment tensor thrust solution (Figure 5) is very similar to that for the model of Ando (1979) shown by Eissler and Kanamori (1987), whereas the pattern for a 1° dipping fault (Figure 5) is almost the same as for their conjectured horizontal point force. The Furumoto and Kovach (1979) model and a similar solution with 3° dip show strong Love wave node variation. There is substantial scatter in the data, as expected for 100-s period signals, and there are questions about clipping of the digital signals at High-Gain Long Period Network stations CTA and KON (Nettles & Ekström, 2004), but overall, the data are compatible with very shallow (≤3°) dip of the fault, similar to the finding for the 2018 event. It is quite plausible that some of the mismatch is due to additional radiation from slumping, giving a composite source radiation (e.g., Kawakatsu, 1989; Ma et al., 1999). We infer that the 2018 event reruptured a portion of the 1975 rupture zone.

Long-period surface wave spectra provide strong sensitivity to dip for shallow, shallowly dipping dip-slip faulting and can help to identify the geometry of structures that rupture in near-trench tsunami earthquakes and on basal décollement. As routine long-period moment tensor inversions are commonly performed using complete waveforms, the nodal behavior for Love waves is intrinsically not as evident as in spectral analysis. Low signal-to-noise, phase instability, and associated limited sampling of the nodal directions due to signal-quality criteria may suppress the information about dip, which is concentrated in the subtle nodal asymmetry of Love wave radiation for dip less than about 10°. This information can readily be extracted by conventional surface wave spectral analysis. While long-period spectral information does have limitations for resolving source properties, and complete waveform information is certainly the primary data to use for routine source analyses, the spectral data provide particular sensitivity for shallowly dipping sources of large events. This, in turn, has significant implications for tectonic interpretations, as the Love wave observations can convincingly exclude significant slip on splay faults, if very low dip angle is indeed preferred.

Acknowledgments
The Incorporated Research Institutions for Seismology (IRIS) data management service (DMS) (http://www.iris.edu/hq/) was used to access the long-period (LH) seismic data from Global Seismic Network and Federation of Digital Seismic Network stations. Two anonymous reviewers provided helpful comments on the manuscript. This work was supported by NSF grant EAR1802364 to Thorne Lay and the junior Thousand Talents Plan of China and the 100 Talents program of Sun Yat-sen University to Lingling Ye.

References

Ammon, C. J., Kanamori, H., Lay, T., & Velasco, A. A. (2006). The 17 July 2006 Java tsunami earthquake. *Geophysical Research Letters*, *33*, L14314. https://doi.org/10.1029/2006GL026303

Ando, M. (1979). The Hawaii earthquake of November 29, 1975: Low dip angle faulting due to forceful injection of magma. *Journal of Geophysical Research*, *84*(B13), 7616–7626. https://doi.org/10.1029/JB084iB13p07616

Bai, Y., Ye, L., Yamazaki, Y., Lay, T., & Cheung, K. F. (2018). The 4 May 2018 M_W 6.9 Hawaii Island earthquake and implications for tsunami hazards. *Geophysical Research Letters*, *45*. https://doi.org/10.1002/2018GL079742

Bilek, S. L., & Lay, T. (2002). Tsunami earthquakes possibly widespread manifestations of frictional conditional stability. *Geophysical Research Letters*, *29*(14), 1673. https://doi.org/10.1029/2002GL015215

Dahlen, F. A. (1993). Single-force representation of shallow landslide sources. *Bulletin of the Seismological Society of America*, *83*(1), 130–143.

Day, S. J., Watts, P., Grilli, S. T., & Kirby, J. T. (2005). Mechanical models of the 1975 Kalapana, Hawaii earthquake and tsunami. *Marine Geology*, *215*(1-2), 59–92. https://doi.org/10.1016/j.margeo.2004.11.008

Delaney, P. T., Denlinger, R. P., Lisowski, M., Miklius, A., Okubo, P. G., Okamura, A. T., & Sako, M. K. (1998). Volcanic spreading at Kilauea, 1976–1996. *Journal of Geophysical Research*, *103*(B8), 18,003–18,023. https://doi.org/10.1029/98JB01665

Denlinger, R. P., & Okubo, P. (1995). Structure of the mobile south flank of Kilauea volcano, Hawaii. *Journal of Geophysical Research*, *100*(B12), 24,499–24,507. https://doi.org/10.1029/95JB01479

Duputel, Z., Rivera, L., Kanamori, H., & Hayes, G. (2012). *W* phase source inversion for moderate to large earthquakes (1990–2010). *Geophysical Journal International*, *189*(2), 1125–1147. https://doi.org/10.1111/j.1365-246X.2012.05419.x

Dziewonski, A. M., & Anderson, D. L. (1981). Preliminary reference Earth model. *Physics of the Earth and Planetary Interiors*, *25*(4), 297–356. https://doi.org/10.1016/0031-9201(81)90046-7

Eissler, H. K., & Kanamori, H. (1987). A single-force model for the 1975 Kalapana, Hawaii, earthquake. *Journal of Geophysical Research*, *92*(B6), 4827–4836. https://doi.org/10.1029/JB092iB06p04827

Furumoto, A. S., & Kovach, R. L. (1979). The Kalapana earthquake of November 29, 1975: An intra-plate earthquake and its relation to geothermal processes. *Physics of the Earth and Planetary Interiors*, *18*(3), 197–208. https://doi.org/10.1016/0031-9201(79)90114-6

Gillard, D., Wyss, M., & Okubo, P. (1996). Type of faulting and orientation of stress and strain as a function of space and time in Kilauea's south flank, Hawaii. *Journal of Geophysical Research*, *101*(B7), 16,025–16,042. https://doi.org/10.1029/96JB00651

Hayes, G. P., Wald, D. J., & Johnson, R. L. (2012). Slab 1.0: A three-dimensional model of global subduction zone geometries. *Journal of Geophysical Research*, *117*, B01302. https://doi.org/10.1029/2011JB008524

Heidarzadeh, M. (2011). Major tsunami risks from splay faulting. In N.-A. Mörner (Ed.), *The tsunami threat—Research and technology* (Chap. 5, pp. 67–80). Croatia: InTech.

Hill, E. M., Borrero, J. C., Huang, Z., Qiu, Q., Banerjee, P., Natawidjaja, D. H., et al. (2012). The 2010 M_W 7.8 Mentawai earthquake: Very shallow source of a rare tsunami earthquake determined from tsunami field survey and near-field GPS data. *Journal of Geophysical Research*, *117*, B064502. https://doi.org/10.1029/2012JB009159

Kanamori, H. (1972). Mechanism of tsunami earthquakes. *Physics of the Earth and Planetary Interiors*, *6*(5), 346–359. https://doi.org/10.1016/0031-9201(72)90058-1

Kanamori, H., & Given, J. W. (1981). Use of long-period surface waves for rapid determination of earthquake-source parameters. *Physics of the Earth and Planetary Interiors*, *27*(1), 8–31. https://doi.org/10.1016/0031-9201(81)90083-2

Kanamori, H., & Given, J. W. (1982). Analysis of long-period seismic waves excited by the May 18, 1980 eruption of Mount St. Helens—A terrestrial monopole? *Journal of Geophysical Research*, *87*(B7), 5422–5432. https://doi.org/10.1029/JB087iB07p05422

Kawakatsu, H. (1989). Centroid single force inversion of seismic waves generated by landslides. *Journal of Geophysical Research*, *94*(B9), 12,363–12,374. https://doi.org/10.1029/JB094iB09p12363

Lay, T., Ammon, C. J., Kanamori, H., Yamazaki, Y., Cheung, K. F., & Hutko, A. R. (2011). The 25 October 2010 Mentawai tsunami earthquake (M_W 7.8) and the tsunami hazard presented by shallow megathrust ruptures. *Geophysical Research Letters*, *38*, L06302. https://doi.org/10.1029/2010GL046552

Liu, C., Lay, T., & Xiong, X. (2018). Rupture in the 4 May 2018 M_W6.9 earthquake seaward of the Kilauea east rift zone fissure eruption in Hawaii. *Geophysical Research Letters*, *45*. https://doi.org/10.1029/2018GL079349

Ma, K.-F., Kanamori, H., & Satake, K. (1999). Mechanism of the 1975 Kalapana, Hawaii, earthquake inferred from tsunami data. *Journal of Geophysical Research*, *104*(B6), 13,153–13,167. https://doi.org/10.1029/1999JB900073

Morgan, J. K., Moore, G. F., & Clague, D. A. (2003). Slope failure and volcanic spreading along the submarine south flank of Kilauea volcano, Hawaii. *Journal of Geophysical Research*, *108*(B9), 2415. https://doi.org/10.1029/2003JB002411

Morgan, J. K., Moore, G. F., Hills, D. J., & Leslie, S. (2000). Overthrusting and sediment accretion along Kilauea's mobile south flank, Hawaii: Evidence for volcanic spreading from marine seismic reflection data. *Geology*, *28*(7), 667–700. https://doi.org/10.1130/0091-7613(2000)28<667:OASAAK>2.0.CO;2

Nettles, M., & Ekström, G. (2004). Long-period source characteristics of the 1975 Kalapana, Hawaii, earthquake. *Bulletin of the Seismological Society of America*, *94*(2), 422–429. https://doi.org/10.1785/0120030090

Newman, A. V., Hayes, G., Wei, Y., & Convers, J. (2011). The 25 October 2010 Mentawai tsunami earthquake, from real-time discriminants, finite-fault rupture, and tsunami excitation. *Geophysical Research Letters*, *38*, L05302. https://doi.org/10.1029/2010GL046498

Park, J., Morgan, J. K., Zelt, C. A., Okubo, P. G., Peters, L., & Benesh, N. (2007). Comparative velocity structure of active Hawaiian volcanoes from 3-D onshore-offshore seismic tomography. *Earth and Planetary Science Letters*, *259*, 500–516.

Park, J.-O., Tsuru, T., Kodaira, S., Cummins, P. R., & Kaneda, Y. (2002). Splay fault branching along the Nankai subduction zone. *Science*, *297*(5584), 1157–1160. https://doi.org/10.1126/science.1074111

Plaza-Faverola, A., Henrys, S., Pecher, I., Wallace, L., & Klaeschen, D. (2016). Splay fault branching from the Hikurangi subduction shear zone: Implications for slow slip and fluid flow. *Geochemistry, Geophysics, Geosystems*, *17*, 5009–5023. https://doi.org/10.1002/2016GC006563

Polet, J., & Kanamori, H. (2000). Shallow subduction zone earthquakes and their tsunamigenic potential. *Geophysical Journal International*, *142*(3), 684–702. https://doi.org/10.1046/j.1365-246x.2000.00205.x

Satake, K., Nishimura, Y., Putra, P. S., Gusman, A. R., Sunendar, H., Fujii, Y., et al. (2013). Tsunami source of the 2010 Mentawai, Indonesia earthquake inferred from tsunami field survey and waveform modeling. *Pure and Applied Geophysics*, *170*(9-10), 1567–1582. https://doi.org/10.1007/s00024-012-0536-y

Singh, S. C., Hananto, N., Mukti, M., Permana, H., Djajadihardja, Y., & Harjono, H. (2011). Seismic images of the megathrust rupture during the 25th October 2010 Pagai earthquake, SW Sumatra: Frontal rupture and large tsunami. *Geophysical Research Letters*, *38*, L16313. https://doi.org/10.1029/2011GL048935

Swanson, D. A., Duffield, W. A., & Fiske, R. S. (1976). Displacement of the south flank of Kilauea volcano: The result of forceful intrusion of magma into the rift zones. *Geological Survey Professional Paper*, *963*, 44.

Velasco, A. A., Lay, T., & Zhang, J. (1992). Improved resolution of earthquake source parameters from long-period surface wave inversions. *Physics of the Earth and Planetary Interiors*, *74*(3-4), 101–107. https://doi.org/10.1016/0031-9201(92)90002-D

Wyss, M. (1988). A proposed source model for the great Kau, Hawaii, earthquake of 1868. *Bulletin of the Seismological Society of America*, *78*(4), 1450–1462.

Wyss, M., & Kovach, R. L. (1988). Comment on "A single-force model for the 1975 Kalapana, Hawaii earthquake" by Holly K. Eissler and Hiroo Kanamori. *Journal of Geophysical Research*, *93*(B7), 8078–8082. https://doi.org/10.1029/JB093iB07p08078

Yue, H., Lay, T., Rivera, L., Bai, Y., Yamazaki, Y., Cheung, K. F., et al. (2014). Rupture process of the 2010 M_W 7.8 Mentawai tsunami earthquake form joint inversion of near-field hr-GPS and teleseismic body wave recordings constrained by tsunami observations. *Journal of Geophysical Research: Solid Earth*, *119*, 5574–5593. https://doi.org/10.1002/2014JB011082

Zhang, J., & Lay, T. (1990). Source parameters of the 1989 Loma Prieta earthquake determined from long-period Rayleigh waves. *Geophysical Research Letters*, *17*(8), 1195–1198. https://doi.org/10.1029/GL017i008p01195